



ARTICLE

Inhibition of the $I_{Na/K}$ and the activation of peak I_{Na} contribute to the arrhythmogenic effects of aconitine and mesaconitine in guinea pigs

Xiang-chong Wang^{1,2,3}, Qing-zhong Jia^{1,2}, Yu-lou Yu^{1,2}, Han-dong Wang^{1,2}, Hui-cai Guo⁴, Xin-di Ma^{1,2}, Chun-tong Liu^{1,2}, Xue-yan Chen^{1,2}, Qing-feng Miao^{1,2}, Bing-cai Guan^{1,2}, Su-wen Su^{1,2}, He-ming Wei⁵ and Chuan Wang^{1,2}

Aconitine (ACO), a main active ingredient of *Aconitum*, is well-known for its cardiotoxicity. However, the mechanisms of toxic action of ACO remain unclear. In the current study, we investigated the cardiac effects of ACO and mesaconitine (MACO), a structurally related analog of ACO identified in *Aconitum* with undocumented cardiotoxicity in guinea pigs. We showed that intravenous administration of ACO or MACO (25 µg/kg) to guinea pigs caused various types of arrhythmias in electrocardiogram (ECG) recording, including ventricular premature beats (VPB), atrioventricular blockade (AVB), ventricular tachycardia (VT), and ventricular fibrillation (VF). MACO displayed more potent arrhythmogenic effect than ACO. We conducted whole-cell patch-clamp recording in isolated guinea pig ventricular myocytes, and observed that treatment with ACO (0.3, 3 µM) or MACO (0.1, 0.3 µM) depolarized the resting membrane potential (RMP) and reduced the action potential amplitude (APA) and durations (APDs) in a concentration-dependent manner. The ACO- and MACO-induced AP remodeling was largely abolished by an I_{Na} blocker tetrodotoxin (2 µM) and partly abolished by a specific Na^+/K^+ pump (NKP) blocker ouabain (0.1 µM). Furthermore, we observed that treatment with ACO or MACO attenuated NKP current ($I_{Na/K}$) and increased peak I_{Na} by accelerating the sodium channel activation with the EC_{50} of 8.36 ± 1.89 and 1.33 ± 0.16 µM, respectively. Incubation of ventricular myocytes with ACO or MACO concentration-dependently increased intracellular Na^+ and Ca^{2+} concentrations. In conclusion, the current study demonstrates strong arrhythmogenic effects of ACO and MACO resulted from increasing the peak I_{Na} via accelerating sodium channel activation and inhibiting the $I_{Na/K}$. These results may help to improve our understanding of cardiotoxic mechanisms of ACO and MACO, and identify potential novel therapeutic targets for *Aconitum* poisoning.

Keywords: aconitine; mesaconitine; arrhythmia; action potential; Na^+/K^+ pump current; voltage-gated sodium channel current

Acta Pharmacologica Sinica (2021) 42:218–229; <https://doi.org/10.1038/s41401-020-0467-6>

INTRODUCTION

Aconitum, a Chinese herbal medicine, has been widely used for over 2000 years to treat various diseases, such as rheumatoid arthritis, heart failure, gastroenteritis, bronchial asthma, and various tumors [1]. However, *Aconitum* has been associated with high neurotoxicity and cardiotoxicity, which severely limits its clinical use [2]. Aconitine (ACO), a highly toxic diterpenoid alkaloid obtained from the plant *Aconitum* genus, has been recognized for its phytomedicine effects on the central nervous system, heart, and skeletal muscle [3]. However, ACO has also demonstrated arrhythmogenic effects, including the induction of ventricular premature beats (VPBs), atrioventricular blockade (AVB), ventricular tachycardia (VT), ventricular fibrillation (VF), torsade de pointes, and sudden death in a dose-dependent manner [4]. The reproducible and durable arrhythmogenic effects of ACO have

made it a reagent for creating a classic model of arrhythmias in experimental animals [4, 5]. However, the mechanisms by which ACO induces arrhythmia remain unclear. At the cellular level, reports showed that ACO could prolong action potential durations (APDs) and induce early and delayed after-depolarization (EAD and DAD, respectively) and triggered activity (TA) [5–7]. Such AP remodeling was associated with an increase in late sodium channel current (late I_{Na}) caused by abnormal opening of voltage-gated cardiac Na^+ channels during repolarization (phase 3) [7, 8]. However, other mechanisms may also be involved. ACO has been reported to disrupt intracellular Ca^{2+} homeostasis [9–11], suppress L-type Ca^{2+} channel currents (I_{Ca-L}) [10], and inhibit human ether-a-go-go-related gene K^+ channels and ultrarapid-delayed rectifier K^+ currents (I_{kur}) [6, 7]. A recent study showed that the outward current induced by the Na^+/K^+ pump current ($I_{Na/K}$) is one of the

¹Department of Pharmacology, The Key Laboratory of Pharmacology and Toxicology for New Drugs, Hebei Medical University, Shijiazhuang 050017, China; ²The Key Laboratory of Neural and Vascular Biology, Ministry of Education, Hebei Medical University, Shijiazhuang 050017, China; ³Department of Pharmacology, Hebei Key Laboratory of Chinese Medicine Research on Cardio-cerebrovascular Disease, Hebei Higher Education Institute Applied Technology Research Center on TCM Formula Preparation, Hebei University of Chinese Medicine, Shijiazhuang 050091, China; ⁴Department of Toxicology, Hebei Medical University, Shijiazhuang 050017, China and ⁵Research Laboratory, KK Women's & Children's Hospital, Singapore 229899, Singapore

Correspondence: Su-wen Su (suswmk@hebmu.edu.cn) or He-ming Wei (wei.heming@khh.com.sg) or Chuan Wang (wangchuan@hebmu.edu.cn)

These authors contributed equally: Xiang-chong Wang, Qing-zhong Jia

Received: 29 December 2019 Accepted: 23 June 2020

Published online: 3 August 2020

most important determinants of repolarization abnormality susceptibility [12]. In addition, a report demonstrated that the increment of peak I_{Na} contributed to the upstroke of fast APs (phase 0) of cardiac myocytes [13]. Nevertheless, the effects of ACO on peak I_{Na} , $I_{Na/K}$, and intracellular Ca^{2+} concentration ($[Ca^{2+}]_i$) in guinea pig ventricular myocytes are still unknown.

Mesaconitine (MACO) is a structurally related analog of ACO and is pharmacologically the most active component from *Aconitum*, with various pharmacological effects, such as analgesia and the relaxation of rat aorta [14, 15]. However, the arrhythmogenic effects of MACO remain largely unexplored. Understanding the arrhythmogenic mechanisms of ACO and MACO could lead to the identification of novel therapeutic targets for *Aconitum*-induced arrhythmias and proper uses of ACO-induced arrhythmia models in pharmacology research.

In the present study, we compared the arrhythmogenic effects of ACO and MACO in guinea pigs *in vivo* and explored the underlying mechanisms *in vitro*. We confirmed that ACO and MACO induced various types of arrhythmias by electrocardiogram (ECG) recording *in vivo* and shortened APDs; positively shifted the resting membrane potential (RMP); and induced EAD, DAD, and TA *in vitro*. ACO- and MACO-induced AP changes were associated with intracellular Ca^{2+} overload following the elevation of intracellular Na^+ concentration ($[Na^+]_i$), induced by $I_{Na/K}$ inhibition and the peak I_{Na} increment through the acceleration of sodium channel activation.

MATERIALS AND METHODS

Chemicals and drugs

ACO, MACO, and amphotericin B were purchased from Sigma-Aldrich (St. Louis, MO, USA). They were prepared as stock solutions by dissolving in dimethylsulfoxide (DMSO) and diluting to the final concentration with external or internal solution before the start of the experiment. The final concentration of DMSO was less than 0.01%, which does not affect peak I_{Na} , $I_{Na/K}$, or APs. Tetrodotoxin (TTX, Sigma-Aldrich) was also prepared as a stock solution by dissolving it in distilled water and was stored at $-80^\circ C$. OUA (Sigma-Aldrich) was simply added to the external solution before the experiments. Type II collagenase was purchased from Worthington Biochem, Freehold, NJ, USA. Nimodipine and RIPA lysis buffer were purchased from Thermo Fisher Scientific, Rockford, IL, USA. Fluo-4 AM was purchased from Invitrogen, Carlsbad, CA, USA.

Animals

Male guinea pigs (Hartly, 300–350 g) were obtained from the Experimental Animal Center of Hebei Medical University. The uses of experimental animals were approved by the Institutional Animal Care and Use Committee of Hebei Medical University. This investigation conformed to the Guidelines for the Care and Use of Laboratory Animals and followed the approval of the Bioethical Committee of Hebei Medical University.

ECG recordings

The ECG recordings were performed on 25 male guinea pigs weighing 300–350 g. The animals were randomly assigned into three groups: the saline control group ($n = 5$, to reduce the number of animals used), the ACO group (25 $\mu g/kg$ group, $n = 10$), and the MACO group (25 $\mu g/kg$ group, $n = 10$). After weighing, the animals were anesthetized by intraperitoneal injection with 1.2% sodium pentobarbital at a dosage of 3 mL/kg [11]. After 10 min of stabilization, 25 $\mu g/kg$ ACO or MACO was administered as a bolus injection through the femoral vein. The dosages of ACO and MACO were determined based on previous studies [4, 5] and our preliminary experiment. Normal saline solution (1.0 mL/kg) was given to the control animals. Next, the standard lead II ECGs were continuously recorded using a computerized Bipoc System

(RM6240, Chengdu, China) for 120 min before and after the administration of ACO, MACO, or normal saline. Arrhythmias were evaluated according to the diagnostic criteria advocated by the Lambeth Convention [16]. After recordings, the time of the first occurrence (onset time) and the incidence (the rate of occurrence) of various arrhythmias in each group were analyzed. Finally, the time to death of each animal and mortality in each group were calculated.

Isolation of single ventricular myocytes

Single ventricular myocytes were enzymatically dissociated from the hearts of healthy adult guinea pigs (300–350 g) as described previously [17] but with slight modification. Using a Langendorff retrograde apparatus, the isolated hearts were perfused retrogradely with Ca^{2+} -free cold Tyrode's solution composed of (in mM) NaCl, 140; KCl, 5.4; $MgCl_2$, 1.0; HEPES, 10; and glucose, 10 (pH 7.4, adjusted with NaOH) for 5 min, and then the solution was switched to one containing 0.4 mg/mL type II collagenase and continually perfused for 12–15 min. Next, the left ventricular free wall was cut into small pieces in a high- K^+ solution composed of (in mM) KOH, 80; KCl, 40; KH_2PO_4 , 25; $MgSO_4$, 3; glutamic acid, 50; taurine, 20; HEPES, 10; EGTA, 1; and glucose, 10 (adjusted to pH 7.2 with KOH). Cells were harvested, and only those exhibiting a rod-shaped morphology were used for electrophysiological recording within 6–8 h after isolation.

Electrophysiological recordings

Patch pipettes were fabricated from glass capillaries (OD, 1.5 mm; ID, 0.9 mm, Warner Instrument Co.) using a Sutter P-97 microelectrode puller (Sutter Instrument, Novato, USA). The tips were then heat polished with an MF-900 microforge (Narishige, Tokyo, Japan). When filled with the standard pipette solution, the pipettes had a resistance of 2–4 M Ω . All experiments were performed at the room temperature (22–25 $^\circ C$). After patching into a myocyte in a whole-cell configuration, the membrane potential was measured with an Axoclamp 700B amplifier (Axon Instrument Inc., Foster City, USA). The electrical signals were sampled at 2.5–10 kHz, filtered at 2 kHz using a low-pass filter and digitized with an A/D converter (Digidata 1440 A; Axon Instruments). pClamp software (Version 8.1; Axon Instrument) was used to generate voltage-pulse protocols and acquire and analyze data.

The cell suspension was placed on the microscopic groove. The amphotericin B (250 $\mu g/mL$) perforated patch-clamp technique was used to record the APs in the current-clamp mode [17, 18]. Pipette solution contained (in mM) potassium glutamate, 120; KCl, 25; $MgCl_2$, 1; $CaCl_2$, 1; and HEPES, 10 (pH 7.2 adjusted with KOH). The external solution contained (in mM) NaCl, 138; KCl, 4; $MgCl_2$, 1; $CaCl_2$, 2; NaH_2PO_4 , 0.33; glucose, 10; HEPES, 10 (pH 7.4 adjusted with NaOH). APs were evoked with a supra-threshold (2000 pA) current pulse of ~4–6-ms duration at a rate of 1 Hz. Then, the parameters of APs, including RMP, APA, APD_{30} , APD_{50} , and APD_{90} , were analyzed before and after the treatment of the myocytes with ACO or MACO at different concentrations [17, 18]. The concentrations of ACO (0.3, 3 μM) were selected based on a previous study [5] and our preliminary experiments. For MACO, since it has similar yet more potent effects than ACO, relatively lower concentrations (0.1, 0.3 μM) were adopted.

Peak I_{Na} was recorded according to the method described previously with some modifications [19]. The patch pipettes were backfilled with a Cs^+ -rich internal solution containing (in mM) CsCl, 120; $MgCl_2$, 5; $CaCl_2$, 1; Na_2ATP , 5; EGTA, 11; and HEPES, 10 (pH 7.4 adjusted with CsOH). The external solution contained (in mM) choline chloride, 130; CsCl, 5.4; $CaCl_2$, 1; $MgCl_2$, 1; NaH_2PO_4 , 0.33; HEPES, 10; NaCl, 20; and nimodipine, 0.01 (pH 7.3 adjusted with CsOH). As peak I_{Na} is fast and large, special conditions were necessary to record it quantitatively. Patch pipettes with low resistance (1.5–2.5 M Ω) were used to facilitate the dialysis of cells with the pipette solution and to minimize voltage errors. Cs^+ -based

external and internal solutions containing similar levels of Na^+ were used to reduce the gradient for Na^+ entry and to block any contamination from the potassium current. In addition, 65%–75% of the series resistance could be compensated [20]. To determine the voltage dependence of steady-state activation, currents were elicited by a 50-ms pulse from a holding potential of -90 mV to test potentials between -100 and 0 mV in 5 mV increments. The Na^+ conductance (G) was calculated by dividing the peak current for each voltage step by the driving force ($V_m - V_{\text{rev}}$) and then normalizing it to the peak conductance (G_{max}). Data were fitted with the Boltzmann equation, $G/G_{\text{max}} = 1/\{1 + \exp[(V_{1/2} - V_m)/k]\}$, in which $V_{1/2}$ was the voltage at which half of the Na^+ channels were activated, k was the slope factor, and V_m was the membrane potential. The steady-state inactivation curves were generated via standard two-pulse protocols: cells were stepped to 50 -ms preconditioning potentials from the holding potential of -90 mV, varying between -120 and -25 mV (prepulse), followed by a 50 -ms test pulse to -20 mV. Currents (I) were normalized to I_{max} and fit to a Boltzmann equation of the form $I/I_{\text{max}} = 1/\{1 + \exp[(V_m - V_{1/2})/k]\}$, in which $V_{1/2}$ was the voltage at which half of the Na^+ channels were inactivated, k was the slope factor, and V_m was the membrane potential. Recovery from inactivation was analyzed by fitting data with the two exponential equations $I(t)/I_{\text{max}} = A_f \times [1 - \exp(-t/\tau_f)] + A_s \times [1 - \exp(-t/\tau_s)]$, where values for A and τ refer to amplitudes and time constants, respectively [19, 21, 22]. Curve fitting and data analysis were performed using Clampfit 10.2 software (Axon Instruments) and Origin 8 (OriginLab Corporation).

The external solution used for recording the $I_{\text{Na/K}}$ contained (in mM) NaCl , 137.7; NaOH , 2.3; MgCl_2 , 1; glucose, 10; HEPES, 5; KCl , 4.6; BaCl_2 , 0.5; and CdCl_2 , 0.2 (pH 7.4, adjusted with HCl or NaOH). The standard pipette solution contained (in mM) sodium aspartic acid, 50; potassium aspartic acid, 20; CsOH , 30; TEACl, 20; HEPES, 5; MgSO_4 , 5; EGTA, 11; glucose, 10; and Na_2GTP , 5 (pH 7.2, adjusted with CsOH). Under the present experimental conditions with selected external and pipette solutions, the membrane current through Ca^{2+} channels, K^+ channels, and $\text{Na}^+/\text{Ca}^{2+}$ exchangers (NCXs) was minimized. K^+ channel currents were suppressed by the addition of CsOH and TEACl to the internal solution and BaCl_2 to the external solution. High-threshold (N-, L-, and P- type) and low-threshold (T- type) calcium channel currents were eliminated by the removal of Ca^{2+} from the external solution, and any residual influx of Ca^{2+} through these voltage-gated Ca^{2+} channels was blocked by the addition of CdCl_2 to the external solution. The Na^+ channels and T-type Ca^{2+} channels were inactivated by setting the holding potential to 0 mV, and the NCX current was blocked by eliminating Ca^{2+} from the external and internal solutions [23]. Usually, the recording was started when the current reached steady-state level within 3–5 min after patch rupture. Under these conditions, membrane currents through Ca^{2+} channels, K^+ channels, and NCXs were mostly blocked, and the $I_{\text{Na/K}}$ was identified as the ouabain (OUA)-sensitive current [24, 25].

Measurements of $[\text{Na}^+]_i$ and $[\text{Ca}^{2+}]_i$

Fresh guinea pig ventricular myocytes were incubated with ACO (0.3, 3 μM) and MACO (0.1, 0.3 μM) at the room temperature for 30 min, and then 500 μM RIPA lysis buffer was added to lyse the cells at 4°C for intracellular ion measurement. The ion extraction was centrifuged at 4°C for 20 min at 12,000 rpm [20, 25]. $[\text{Na}^+]_i$ was measured by an ion-selective electrode with a Na/K/Cl analyzer (Easylate PLUS, Medica Corporation, USA).

$[\text{Ca}^{2+}]_i$ measurement was performed according to a previous report with slight modifications: ventricular myocytes were incubated with 2 μM Fluo-4-acetoxymethyl ester (Fluo-4 AM, Invitrogen, Carlsbad, CA, USA) in normal Tyrode's solution containing 1.8 mM Ca^{2+} for 30 min at the room temperature. Cells were then washed with dye-free normal Tyrode's solution for 15 min for de-esterification. The fluorescence intensity (IF) of ventricular myocytes was detected by confocal microscopy (SP5,

Wetzlar, Germany) using a 488 nm laser for excitation and a 530 nm laser for emission during one experimental process; 60 scans with 0-s intervals were used [9, 11, 26]. Representative fluorescent images were captured at a frames per 8 s before (control) and after the addition of ACO (0.3 or 3 μM) or MACO (0.1 or 0.3 μM) by using 60 mM KCl as a background. The changes in $[\text{Ca}^{2+}]_i$ were expressed as F/F_0 , in which F_0 and F indicated the IF before and after the administration of ACO or MACO, respectively, within 24 s for lower concentrations and within 64 s for higher concentrations.

Statistical analysis

All averaged values presented are means \pm SEMs. Statistical analysis was performed by one-way analysis of variance (ANOVA), followed by Dunnett's multiple comparison test where applicable (SPSS for Windows v11.0). The differences in the parameters before and after treatment were compared using a paired Student's t test. The percentages of occurrence were compared by the χ^2 test or Fisher's exact probability method. Differences were considered significant when $P < 0.05$.

RESULTS

ACO and MACO caused arrhythmic changes in ECG

The ECG of control animals remained largely unchanged within the 120-min recording (Fig. 1a). Next, various types of arrhythmias, including VPBs (Fig. 1b, c), AVB (Fig. 1d), VT (Fig. 1e), and VF (Fig. 1f), were induced by ACO and MACO in the experimental animals, and the typical ECG traces in the presence of ACO are shown in Fig. 1. The onset time of VPBs, AVB, VT, and VF and the time to the death occurred much earlier in the MACO group than in the ACO group ($P < 0.01$). However, the incidences of VPBs, AVB, and VT were not obviously different in these two groups, while the incidences of VF and mortality were significantly higher in the MACO group than in the ACO group ($P < 0.05$ or $P < 0.01$, respectively) (Table 1).

ACO and MACO remodeled the AP configurations in single ventricular myocytes

The effects of ACO and MACO on AP configurations in isolated guinea pig ventricular myocytes were evaluated by the perforated whole-cell patch-clamp technique in current-clamp mode [17, 18], and the results are shown in Fig. 2. Superimposed traces of APs recorded before and after exposure to 0.3 and 3 μM ACO showed that APD_{30} , APD_{50} , and APD_{90} were markedly shortened in a concentration-dependent manner ($P < 0.01$, Fig. 2a, e). DAD (4/7 cells) and TA (7/7 cells) were induced at higher concentrations of ACO (Table 2). Reduced APA and more depolarized RMP were also observed at higher concentrations ($P < 0.05$, Fig. 2a, f). Similar yet more potent effects of MACO (0.1, 0.3 μM) on APs were noticed (Fig. 2b–d, g, h). APDs were shortened in a concentration-dependent manner ($P < 0.01$, Fig. 2b–d, g). Reduced APA and more depolarized RMP were also observed at higher concentrations of MACO ($P < 0.05$, Fig. 2b–d, h). DAD (6/8 cells), EAD (4/8 cells), and TA (8/8 cells) appeared at higher concentrations (Table 2).

Verification of the causative effects of peak I_{Na} increments on AP remodeling induced by ACO and MACO

Previous studies have shown that ACO could promote abnormal activation of late I_{Na} during the repolarization phase [8], leading to increased $[\text{Na}^+]_i$ and subsequent accumulation of $[\text{Ca}^{2+}]_i$ via the activation of the reverse mode of NCXs. However, the roles of peak I_{Na} on AP changes after ACO and MACO treatments in guinea pig ventricular myocytes are still unknown.

TTX, a selective antagonist of the cardiac sodium channel [27], only increased the RMP values compared with the control at

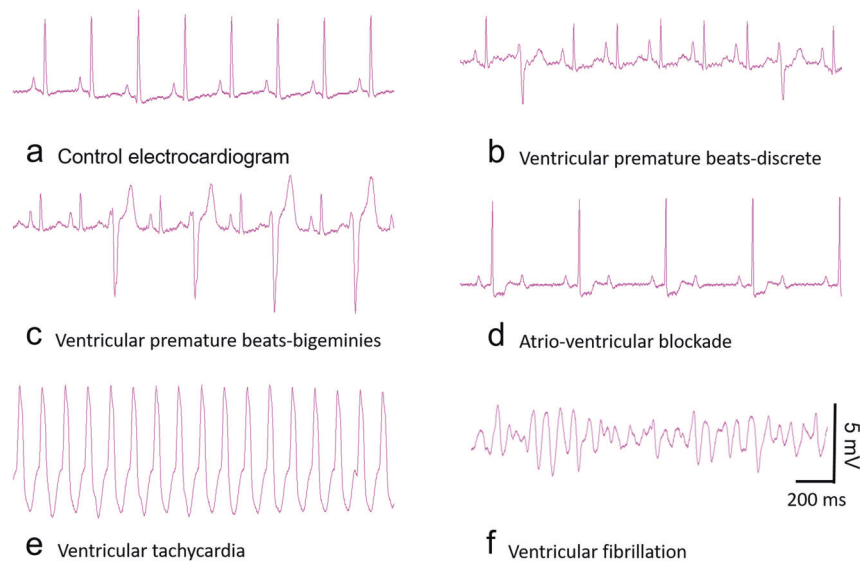


Fig. 1 Typical ECG traces showed various types of ventricular arrhythmias induced by ACO in guinea pigs. The traces were recorded by an RM-6240 multiple-channel ECG recorder (lead II, 50 ms, 20 mV/division). **a** Control ECG tracing. ECG traces of VPBs (**b**, **c**), AVB (**d**), VT (**e**), and VF (**f**) induced by 25 $\mu\text{g}/\text{kg}$ ACO. The ECG traces were chosen from 1 of the 10 independent experiments with ACO treatment. The vertical line indicates 5 mV, and the horizontal line indicates 200 ms. As very similar arrhythmic changes were noticed from MACO (25 $\mu\text{g}/\text{kg}$)-treated guinea pigs, ECG traces of MACO treatment were not shown. Quantitative analysis of the data is shown in Table 1.

Table 1. The onset time and incidence of various arrhythmias and mortality induced by ACO and MACO in guinea pigs.

Type of arrhythmia	ACO group (n = 10)		MACO group (n = 10)	
	Onset time (min)	Incidence	Onset time (min)	Incidence
VPB	22.79 \pm 7.90	8/10	1.46 \pm 0.66**	9/10
AVB	22.75 \pm 13.70	5/10	1.46 \pm 0.66**	8/10
VT	42.30 \pm 15.69	5/10	2.53 \pm 0.87**	9/10
VF	39.65 \pm 7.17	3/10	3.50 \pm 1.19**	9/10*
Mortality	56.32 \pm 11.40	4/10	23.01 \pm 14.92**	10/10**

Incidence is the ratio of animals occurring arrhythmic events or death to the whole animals. The onset time of VPB, AVB, VT, VF, and the death time of the animals in MACO group occurred much earlier than those in ACO group ($P < 0.01$, respectively). However, the incidences of VPB, AVB, and VT had no obvious difference in these two groups, while the incidence of VF and mortality in MACO group were significantly higher than those in ACO group ($P < 0.05$ or $P < 0.01$, respectively).

n number of animals, VPB ventricular premature beats, AVB atrioventricular blockade, VT ventricular tachycardia, VF ventricular fibrillation.

* $P < 0.05$ or ** $P < 0.01$, respectively vs. ACO group.

2 μM ($P < 0.05$), but it largely abolished the changes in AP parameters induced by ACO. The decreased effects of RMP and APA appeared only at ACO 3 μM ($P < 0.05$ or 0.01, respectively) (Fig. 3a, c, d). No DAD or TA were found in the ACO group (Table 2). TTX partly compromised the parameter changes of APs induced by MACO (Fig. 3b, e, f), and the decreased effects of APD, RMP, and APA became obvious only at MACO 0.3 μM ($P < 0.05$ or 0.01, respectively) and rarely EAD (2/8 cells) was found (Table 2). Our data indicate that TTX attenuates the pro-arrhythmic effect of ACO and MACO on guinea pig ventricular myocytes, possibly due to TTX reducing the accumulation of $[\text{Na}^+]_i$ and subsequently the accumulation of $[\text{Ca}^{2+}]_i$, which could result from abnormally activated peak I_{Na} .

ACO and MACO increased peak I_{Na}

Abnormal activation of the cardiac Na^+ channels during phase 3 repolarization and the Na^+ influx increment have been recognized as the dominant mechanism for ACO-induced arrhythmias [8, 28]. However, increased Na^+ influx may also be due to the increase in peak I_{Na} . Therefore, peak I_{Na} was measured in guinea pig ventricular myocytes. Peak I_{Na} was elicited by a 50-ms pulse to -20 mV from the holding potential of -90 mV [19]. Peak I_{Na} was recorded before and after the application of ACO or MACO and 2 μM TTX (Figs. 4a, b and 5a, b). ACO and MACO increased peak I_{Na} in a concentration-dependent manner. Peak I_{Na} was increased by 22.5% \pm 9.2% and 37.2% \pm 9.5% in the presence of ACO 0.3 and 3 μM , respectively (Fig. 4c), while it was increased by 13.0% \pm 1.9% and 26.1% \pm 5.3% in the presence of MACO 0.1 and 0.3 μM , respectively (Fig. 5c). MACO did not show a more potent effect on peak I_{Na} than ACO. The EC_{50} value for ACO was 8.36 \pm 1.89 μM and for MACO was 1.33 \pm 0.16 μM (Figs. 4d and 5d).

Sodium channel gating kinetics were analyzed in the presence of higher concentrations of ACO (100 μM) and MACO (30 μM) (Figs. 4e–k and 5e–k). The concentrations of ACO and MACO achieving 90% maximal activation effects were selected based on the concentration-response relationship curve to observe the most obvious effects. Both ACO and MACO activated peak I_{Na} in a voltage-dependent manner and leftward shifted the activation curve of peak I_{Na} significantly (Figs. 4e–g and 5e–g). Both ACO and MACO decreased the $V_{1/2}$ of activation ($P < 0.01$, Tables 3 and 4). Steady-state inactivation was determined using a standard double-pulse protocol, and the data were fitted by a Boltzmann equation. ACO and MACO did not affect channel inactivation (Figs. 4h, i and 5h, i and Tables 3, 4). Regarding channel recovery from inactivation (Figs. 4j, k and 5j, k), double exponential fits showed that both ACO and MACO accelerated fast component recovery and delayed slow component recovery from inactivation ($P < 0.05$ or $P < 0.01$, respectively) (Tables 3, 4).

Verification of the causative effects of NKP inhibition on arrhythmogenic AP changes induced by ACO and MACO

The NKP plays a crucial role in maintaining the normal electrophysiology of cardiac myocytes, and NKP inhibition is well-known to lead to the accumulation of $[\text{Na}^+]_i$, which subsequently leads to an

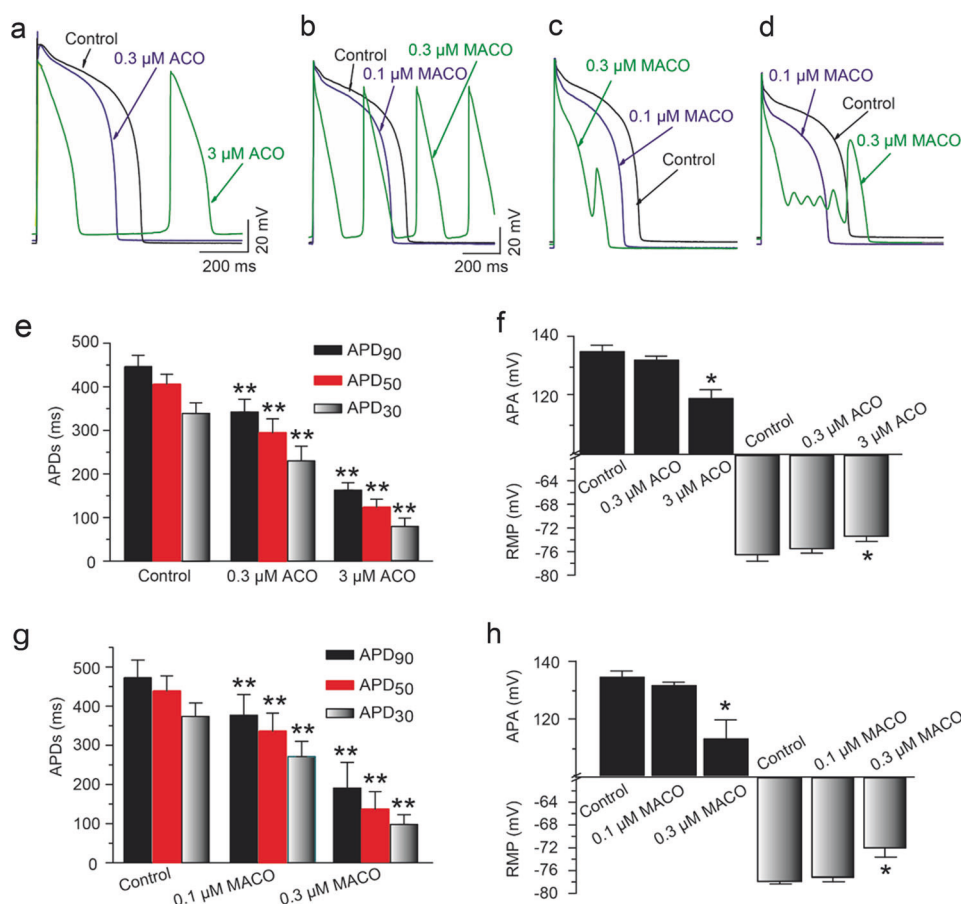


Fig. 2 Effects of ACO and MACO on AP configurations of guinea pig ventricular myocytes. **a** Representative AP waveforms showed shortened APDs and TA by ACO administration. Representative AP waveforms showed shortened APDs (**b–d**) and TA (**b**), EAD (**c**) and DAD (**d**) by MACO administration. Quantitative group data for AP parameters: **e** Concentration-dependent effects of ACO on APD₃₀, APD₅₀, and APD₉₀; **f** Concentration-dependent effects of ACO on APA and RMP; **g** Concentration-dependent effects of MACO on APD₃₀, APD₅₀, and APD₉₀; **h** Concentration-dependent effects of MACO on APA and RMP. There were seven cells from three guinea pig hearts in each group. **P* < 0.05, ***P* < 0.01 vs: control group.

Table 2. Incidence of EAD, DAD, and TA caused by ACO or MACO with or without TTX or OUA

	DAD	TA	MACO	EAD	DAD	TA
ACO	4/7	7/7	MACO	4/8	6/8	8/8
ACO+TTX	0/7*	0/7**	MACO+TTX	2/8	0/8**	0/8**
ACO+OUA	1/8	5/8	MACO+OUA	4/5	1/5	5/5

TTX reduced the incidence of DAD, EAD, or TA caused by ACO or MACO significantly (**P* < 0.05, ***P* < 0.01, respectively). However, OUA had no significant effect on incidence of DAD, EAD, or TA caused by ACO or MACO. The concentrations of ACO, MACO, TTX, and OUA were 3, 0.3, 2, and 0.1 μM, respectively. EAD early after-depolarization, DAD delayed after-depolarization, TA triggered activities.

accumulation of [Ca²⁺]_i via the activation of the reverse mode of NCXs [29, 30]. A recent study showed that the I_{Na/K} was the main contributor to the human repolarization current [12].

To validate whether NKP inhibition is involved in the arrhythmogenic effects of ACO and MACO, OUA was used to block the effects of ACO and MACO on APs. OUA at 0.1 μM shortened APDs and reduced APA and RMP compared with the control (*P* < 0.05 or 0.01, respectively). No further decreased effects were observed after the perfusion of the myocytes with 0.3 μM

ACO, while the decreased effects on APDs and APA again appeared with perfusion with 3 μM ACO (*P* < 0.05 or 0.01, respectively), Fig. 6a, c, d). The reduced effects of MACO (0.1 and 0.3 μM) on AP parameters, including shortened ADPs, remained largely unaffected in the presence of OUA (*P* < 0.05 or 0.01, respectively, Fig. 6b, e, f). DAD (1/8 cells) and TA (5/8 cells) in the ACO group and DAD (1/5 cells), EAD (4/5 cells) and TA (5/5 cells) in the MACO group were observed (Table 2). Our data show that the arrhythmogenic effects of ACO and MACO on APs overlap with those of NKP inhibitors, indicating that both ACO and MACO possess the functional properties of inhibitors of the NKP.

ACO and MACO decreased the I_{Na/K}

As our results indicated that the effects of ACO and MACO on APs collectively resemble those of NKP inhibitors such as OUA and digoxin, the I_{Na/K} was measured in ACO- and MACO-treated ventricular myocytes.

Membrane currents in response to depolarizing (up to +40 mV) and hyperpolarizing (up to -120 mV) test potentials applied from a holding potential of 0 mV by a step of 20 mV were largely time independent and of small amplitude, except for the small amplitude of current relaxations observed at the initial part of hyperpolarizations (Fig. 7a), thus showing that the known ion channel currents in guinea pig ventricular myocytes were largely abolished. The guinea pig ventricular myocytes were then exposed to 100 μM OUA, which caused inward currents at all test potentials, ranging from +40 to -120 mV (Fig. 7b) [23]. Next, the

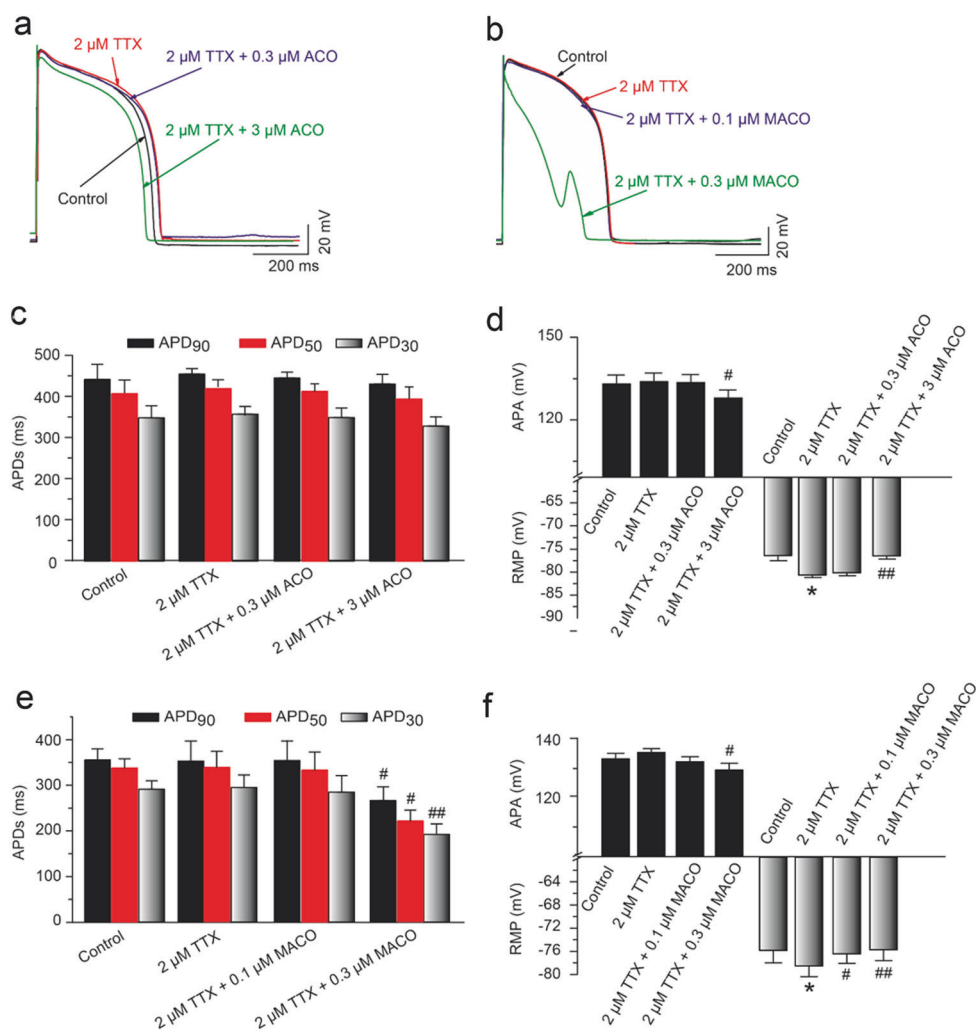


Fig. 3 Effects of ACO and MACO on AP configurations in the presence of TTX in guinea pig ventricular myocytes. Representative waveforms of superimposed APs recorded before and after exposure to TTX and then ACO (a) or MACO (b) in the presence of TTX. Quantitative data for AP parameter measurements in the presence of TTX: **c** Effects of ACO on APD_{30} , APD_{50} and APD_{90} ; **d** Effects of ACO on APA and RMP; **e** Effects of MACO on APD_{30} , APD_{50} , and APD_{90} ; **f** Effects of MACO on APA and RMP. There were seven cells from three guinea pig hearts per group. * $P < 0.05$, vs. control group; # $P < 0.05$, ## $P < 0.01$ vs. TTX group.

$I_{Na/K}$ was determined as the OUA-sensitive current, which was obtained by digitally subtracting the current trace in the presence of OUA from that in its absence at each test potential (Fig. 7c). $I-V$ relationship analysis of the membrane currents was performed in the absence and presence of OUA at the middle part (75 ms) of voltage steps (Fig. 7d). The amplitude of the $I_{Na/K}$ was increased with membrane depolarization from -120 to -20 mV (Fig. 7e) [23, 24], as has been demonstrated in various mammalian cardiac myocytes [31].

To determine whether ACO and MACO inhibit the NKP, the $I_{Na/K}$ was measured by whole-cell patch-clamp recording. A period of ≥ 3 min was required for the pipette, and intracellular contents reached steady state. Next, $100 \mu\text{M}$ OUA was applied, and the holding current shifted inwardly as the $I_{Na/K}$ was blocked (Fig. 7f, h). This change in holding current was considered to reflect the control current and was reversed by the washout of OUA. After washout and once the current had again stabilized, ACO ($0.3 \mu\text{M}$) or MACO ($0.1 \mu\text{M}$) were applied. These applications resulted in an inward shift in holding current due to the inhibition of the $I_{Na/K}$. After a new steady state was achieved, a relatively high concentration of ACO ($3 \mu\text{M}$) or MACO ($0.3 \mu\text{M}$) was applied, which resulted in another inward current shift (Fig. 7f, h). ACO decreased the $I_{Na/K}$ by $26.8\% \pm 4.5\%$ and $48.6\% \pm 14.6\%$ at

concentrations of 0.3 and $3 \mu\text{M}$, respectively (Fig. 7g). A similar inhibitory effect of MACO on the $I_{Na/K}$ was noticed with a higher potency. MACO decreased the $I_{Na/K}$ by $28.0\% \pm 7.5\%$ and $41.8\% \pm 9.3\%$ at concentrations of 0.1 and $0.3 \mu\text{M}$, respectively (Fig. 7i).

ACO and MACO increased $[Na^+]_i$ and $[Ca^{2+}]_i$
The activity of sodium channels and the NKP is closely related to $[Na^+]_i$ and $[Na^+]_i$ -regulated $[Ca^{2+}]_i$ via NCXs has been well-documented [11, 21, 30, 32]. Therefore, the effects of ACO and MACO on $[Na^+]_i$ and $[Ca^{2+}]_i$ were analyzed. Our results showed that both ACO and MACO activated sodium channels and inhibited the NKP, leading to the accumulation of $[Na^+]_i$ and $[Ca^{2+}]_i$. ACO and MACO increased $[Na^+]_i$ in a concentration-dependent manner. $[Na^+]_i$ was increased by $7.5\% \pm 0.6\%$ and $10.8\% \pm 0.7\%$ in the presence of 0.3 and $3 \mu\text{M}$ ACO, respectively (Fig. 8a), while it was increased by $7.8\% \pm 0.9\%$ and $11.3\% \pm 1.1\%$ in the presence of 0.1 and $0.3 \mu\text{M}$ MACO, respectively (Fig. 8b). Subsequently, superimposed Ca^{2+} transients were measured by immunofluorescence in the absence or presence of ACO ($0.3, 3 \mu\text{M}$) and MACO ($0.1, 0.3 \mu\text{M}$), and the myocytes became "round" in response to intracellular Ca^{2+} overload at higher concentrations of ACO and MACO (Fig. 8c). The results showed that ACO and MACO also increased $[Ca^{2+}]_i$ in a concentration-dependent manner (Fig. 8d).

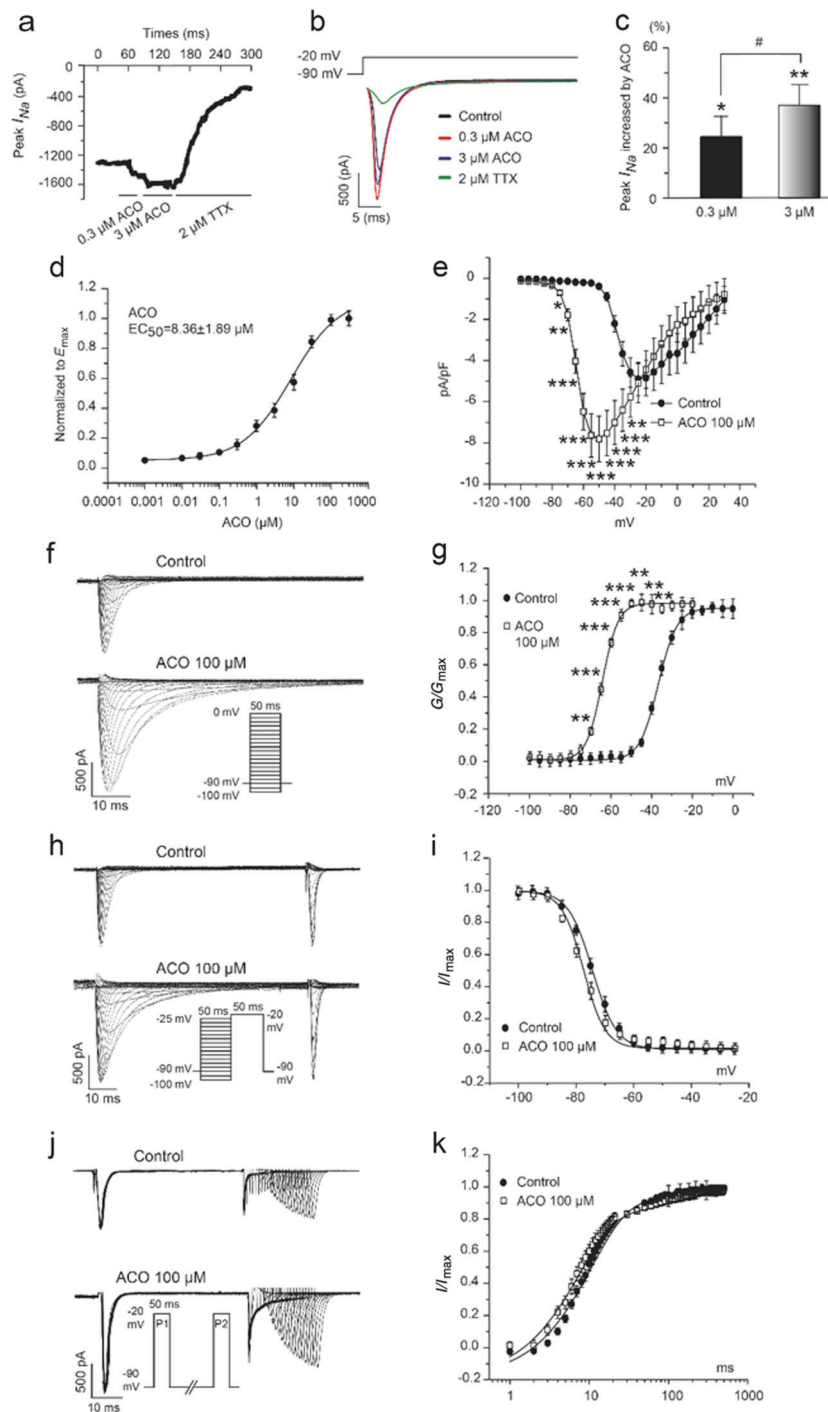


Fig. 4 Effects of ACO on the kinetics of peak I_{Na} in guinea pig ventricular myocytes. **a** The time courses of the peak I_{Na} in the presence of ACO or TTX. **b** Representative traces of peak I_{Na} recorded in the presence of ACO or TTX. The inset shows a schematic of the voltage-clamp protocol. **c** Summarized data of the effects of the percentage increase in ACO on the peak I_{Na} (five cells from three guinea pig hearts in each group). **d** The concentration-response curves of the effects of ACO on peak I_{Na} . The concentration-response relationships were fitted by a logistic function. **e** Summarized data of the I - V relationship of peak I_{Na} after 100 μ M ACO treatment. **f** Typical traces of steady-state activation of peak I_{Na} before and after ACO treatment. The inset shows a schematic of the protocol. **g** Summarized data of steady-state activation of peak I_{Na} . **h** Representative peak I_{Na} traces of steady-state inactivation before and after ACO treatment. The inset shows a schematic of the voltage-clamp protocol. **i** Summarized data of steady-state inactivation curves of peak I_{Na} . **j** Representative peak I_{Na} recovery traces from inactivation in response to voltage commands consisting of two -20 mV depolarization pulses (P1 and P2) from a holding potential of -90 mV, separated by a 1–20-ms or a 20–500-ms variable interval (P1–P2) at -90 mV before and after ACO treatment. The inset shows a schematic of the voltage-clamp protocol. **k** Normalized peak I_{Na} recovery (P2/P1) vs. interpulse interval at -90 mV. There were seven cells from three guinea pig hearts in each group. * $P < 0.05$, ** $P < 0.01$, *** $P < 0.001$ vs. control group; # $P < 0.05$, vs. 0.3 μ M ACO group.

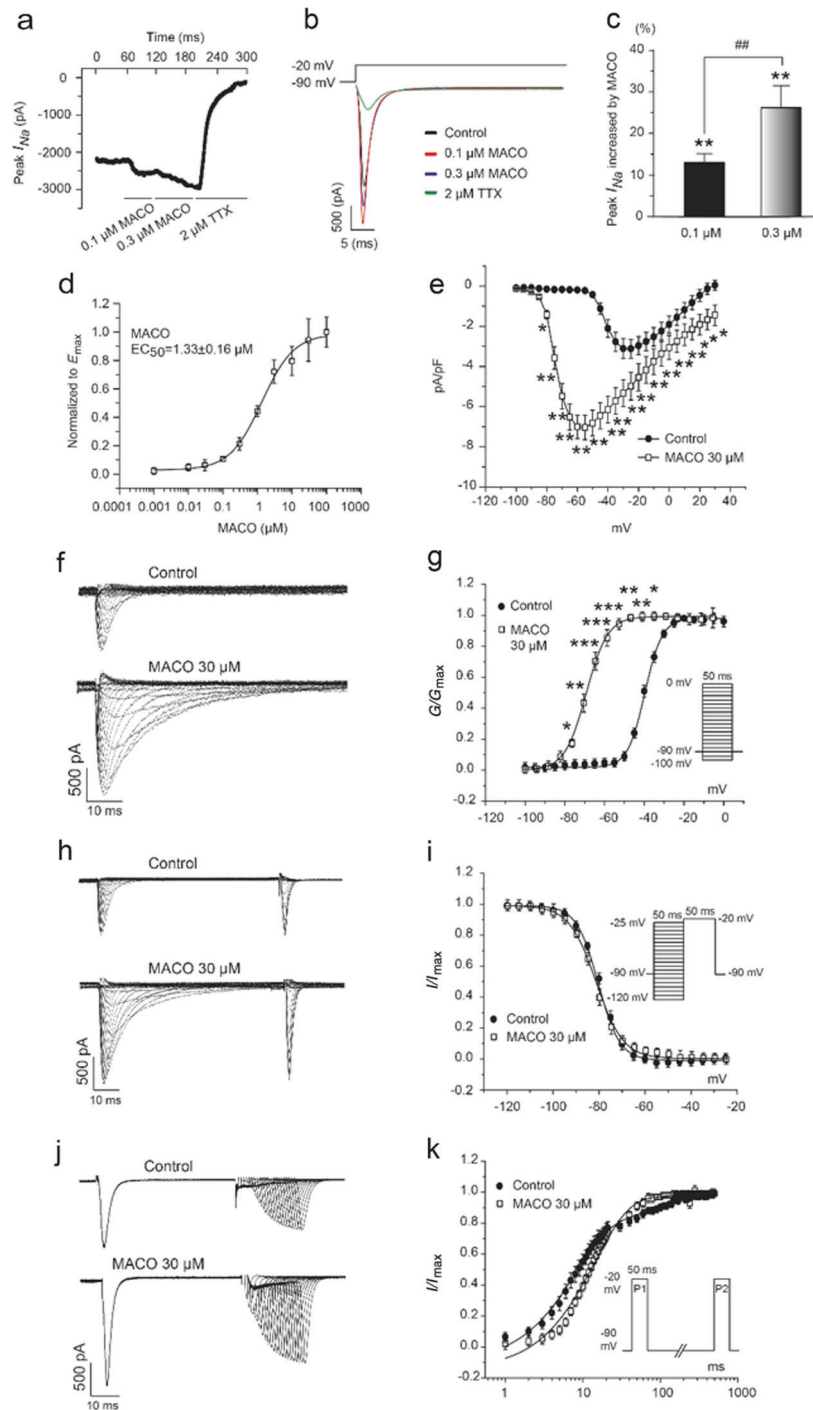


Fig. 5 Effects of MACO on the kinetics of peak I_{Na} in guinea pig ventricular myocytes. **a** The time course of the peak I_{Na} in the presence of MACO or TTX. **b** Typical traces of peak I_{Na} recorded in the presence of MACO or TTX. The inset shows a schematic of the voltage-clamp protocol. **c** Summarized data of the effects of the percentage increase in MACO on the peak I_{Na} . **d** The concentration-response curves of the effects of MACO on peak I_{Na} , where the concentration-response relationships were fitted by the logistic function. **e** Summarized data of the I - V relationship of peak I_{Na} after 30 μ M MACO treatment. **f** Representative peak I_{Na} traces of steady-state activation before and after MACO treatment. The inset shows the schematic of the voltage-clamp protocol. **g** Summarized data of steady-state activation of peak I_{Na} . **h** Representative peak I_{Na} traces of steady-state inactivation before and after MACO treatment. The inset shows a schematic of the voltage-clamp protocol. **i** Summarized data of steady-state inactivation curves of peak I_{Na} . **j** Representative peak I_{Na} recovery traces from inactivation in response to voltage commands consisting of two -20 mV depolarization pulses (P1 and P2) from a holding potential of -90 mV, separated by a 1–20-ms or a 20–500-ms variable interval (P1–P2) at -90 mV before and after MACO treatment. The inset shows the voltage-clamp protocol. **k** Normalized peak I_{Na} recovery (P2/P1) vs. interpulse interval at -90 mV. There were 5–7 cells from three guinea pig hearts in each group. * $P < 0.05$, ** $P < 0.01$, *** $P < 0.001$ vs. control group; ## $P < 0.01$ vs. 0.1 μ M MACO.

DISCUSSION

In the present study, we first confirmed the strong arrhythmogenic effects of ACO and MACO on guinea pigs in vivo, and these

findings were consistent with those of previous reports [4, 5]. We then investigated the mechanism of arrhythmogenic effects with isolated cardiac myocytes in vitro. In ventricular myocytes, ACO-

Table 3. Effects of ACO on the kinetics of I_{Na} .

Parameters	Pre-ACO (n)	Post-100 μ M ACO (n)
$V_{1/2}$ of activation (mV)	-35.51 ± 0.95 (12)	$-63.97 \pm 0.55^{**}$ (12)
k of activation (mV)	5.00 ± 0.39 (12)	$3.77 \pm 0.15^{**}$ (12)
$V_{1/2}$ of inactivation (mV)	-74.24 ± 0.85 (12)	-77.89 ± 1 (12)
k of inactivation (mV)	4.61 ± 0.72 (12)	4.53 ± 0.91 (12)
τ fast recovery (ms)	9.65 ± 0.78 (7)	$6.62 \pm 0.47^{**}$ (6)
τ fast amplitude (%)	86.27 ± 1.55 (7)	85.11 ± 1.89 (6)
τ slow recovery (ms)	90.21 ± 8.12 (7)	$152.43 \pm 12.72^*$ (6)
τ slow amplitude (%)	13.73 ± 1.55 (7)	14.89 ± 1.89 (6)

ACO accelerated the activation and fast recovery of peak I_{Na} , and reduced the slow recovery of peak I_{Na} significantly ($^*P < 0.05$, $^{**}P < 0.01$, respectively vs. pre-ACO group). $V_{1/2}$ half activation/inactivation voltage, k slope factor, τ recovery time consistent, n number of cells.

Table 4. Effects of MACO on the kinetics of I_{Na} .

Parameters	Pre-MACO (n)	Post-30 μ M MACO (n)
$V_{1/2}$ of activation (mV)	-39.48 ± 0.74 (15)	$-74.54 \pm 0.72^{**}$ (15)
k of activation (mV)	4.21 ± 0.36 (15)	3.57 ± 0.24 (15)
$V_{1/2}$ of inactivation (mV)	-79.34 ± 0.97 (15)	-81.34 ± 1.06 (15)
k of inactivation (mV)	4.45 ± 0.14 (15)	4.97 ± 0.31 (15)
τ fast recovery (ms)	11.26 ± 1.32 (7)	$6.32 \pm 0.44^{**}$ (11)
τ fast amplitude (%)	86.82 ± 2.13 (7)	83.43 ± 1.42 (11)
τ slow recovery (ms)	55.45 ± 8.26 (7)	$152.72 \pm 9.03^{**}$ (11)
τ slow amplitude (%)	13.18 ± 1.32 (7)	16.57 ± 1.42 (11)

MACO accelerated the activation and fast recovery of peak I_{Na} , and reduced the slow recovery of peak I_{Na} significantly ($^{**}P < 0.01$ vs. pre-MACO group). $V_{1/2}$ half activation/inactivation voltage, k slope factor, τ recovery time consistent, n number of cells.

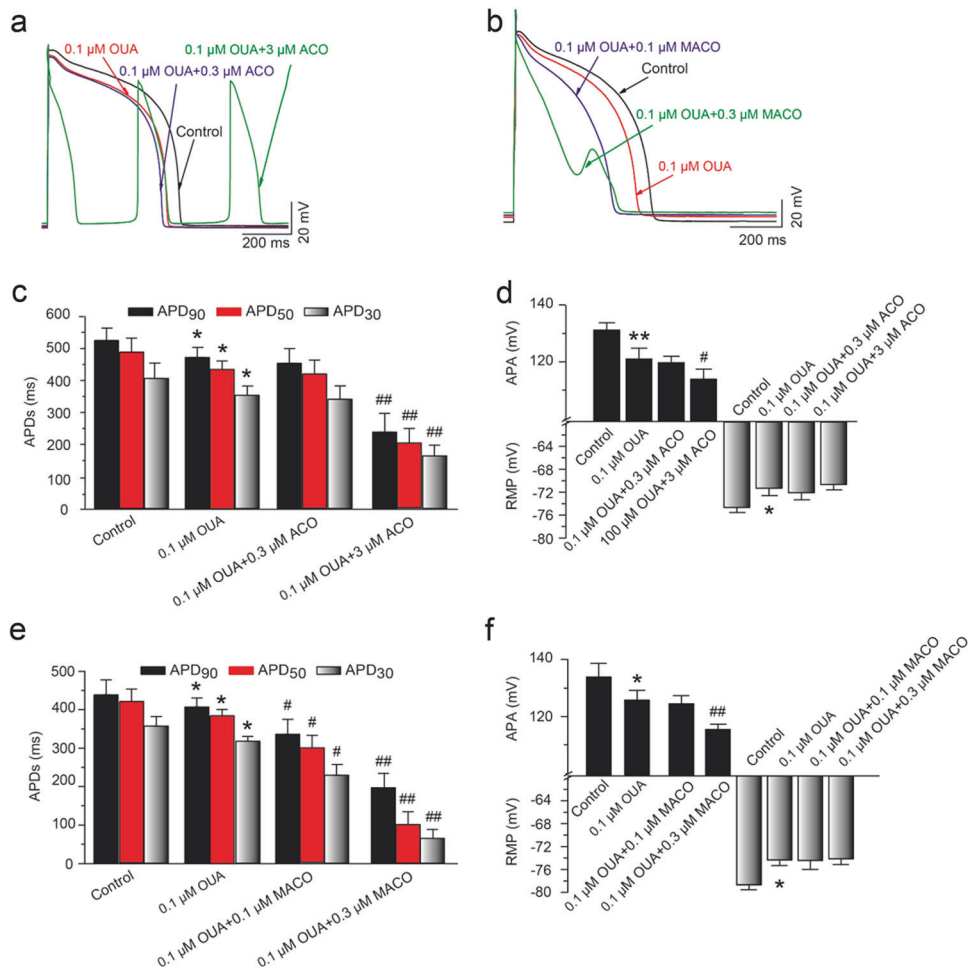


Fig. 6 Effects of ACO or MACO on AP configurations in the presence of OUA in guinea pig ventricular myocytes. **a, b** Typical traces of superimposed APs recorded before and after exposure to OUA and ACO or MACO in the presence of OUA, respectively. Quantitative data for AP parameter measurements in the presence of OUA. **c** Effects of ACO on APD₃₀, APD₅₀, and APD₉₀. **d** Effects of ACO on APA and RMP. **e** Effects of MACO on APD₃₀, APD₅₀, and APD₉₀. **f** Effects of MACO on APA and RMP in the presence of OUA. There were seven cells from three guinea pig hearts in each group. $^*P < 0.05$, $^{**}P < 0.01$ vs. control group; $^{\#}P < 0.05$, $^{\#\#}P < 0.01$ vs. OUA group.

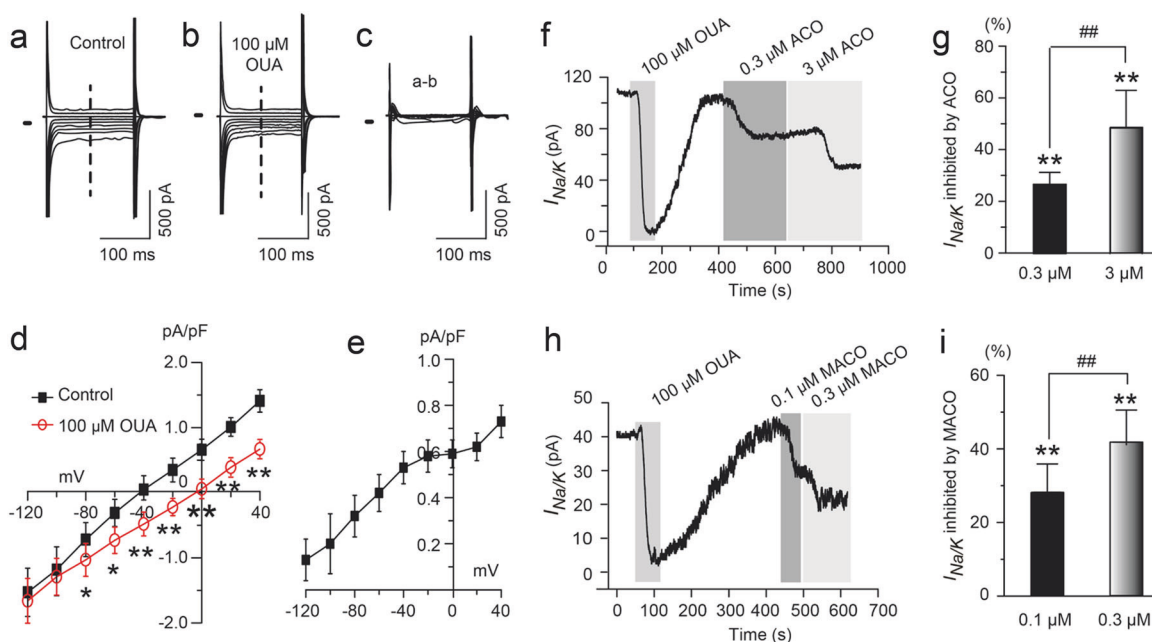


Fig. 7 Effects of ACO and MACO on the $I_{Na/K}$ in guinea pig ventricular myocytes. **a–e** The $I_{Na/K}$ was determined to be an OUA-sensitive component in guinea pig ventricular myocytes. Superimposed current traces in response to 150-ms voltage steps to potential levels between +40 and –120 mV steps applied from a holding potential of 0 mV before (**a**) and 3 min after exposure to 100 μ M OUA (**b**). OUA-sensitive difference currents at test potentials (between +40 and –120 mV) (**c**) were obtained by digital subtraction of the membrane current in the presence of OUA from that in its absence at each test potential. The zero-current level is indicated to the left of the current records by a horizontal line in (**a**), (**b**), and (**c**). **d**, I – V relationship analysis according to the membrane currents at 75 ms (dashed line as shown in (**a**) and (**b**)) measured in the absence and presence of OUA. **e** The I – V relationship for the $I_{Na/K}$ determined as an OUA-sensitive current was derived from the data subtraction of (**d**). **f–i** The $I_{Na/K}$ was inhibited by ACO and MACO in a concentration-dependent manner. The time course of the $I_{Na/K}$ in the presence of OUA, ACO, or MACO is shown in (**f**, **h**), the percentage inhibition of the $I_{Na/K}$ by ACO at 0.3 and 3 μ M is shown in (**g**), and the percentage inhibition of the $I_{Na/K}$ by MACO at 0.1 and 0.3 μ M is shown in (**i**). There were five cells from three guinea pig hearts in the ACO group and six cells from three guinea pig hearts in the MACO group. ** $P < 0.01$, vs. control; ## $P < 0.01$, between treatments.

and MACO-induced changes in APs, including more depolarized RMP, reduced APA, and shortened APDs, in a concentration-dependent manner and frequent occurrences of EAD, DAD, and TA at relatively high concentrations. The changes in APs were largely abolished by TTX, which reconciled in ACO- and MACO-induced AP remodeling. Subsequent observations indicated that the abnormal APs induced by ACO and MACO were associated with elevated intracellular Na^+ -induced Ca^{2+} overload by increasing the peak I_{Na} through the acceleration of sodium channel activation and the inhibition of the NKP. In addition to the abnormal activation of late I_{Na} during repolarization, our data suggest that Na^+ influx might also be achieved by inhibiting the NKP or increasing peak I_{Na} by affecting the channel kinetics, which represents different mechanisms for ACO-induced arrhythmias.

While the dominant mechanism for the arrhythmogenic effects of ACO is the abnormal increase in late I_{Na} during phase 3 repolarization, which is likely attributed to Ca^{2+} overload by triggering the reverse mode of NCXs, leading to EAD, DAD, and TA in APs and eventually inducing arrhythmia [8, 28, 30], our data demonstrate that increased peak I_{Na} and subsequent AP remodeling induced by ACO and MACO could also play a role. This notion is consistent with the report that EAD and DAD occurred when $[Na^+]_i$ increased [33]. Na^+ influx by increasing peak I_{Na} may increase cytosolic Na^+ and induce Ca^{2+} overload via reverse-mode NCXs. However, it remains unclear whether the increase in peak I_{Na} by ACO and MACO observed in the current study and the well-documented ACO-induced increase in late I_{Na} are related. It remains unclear to what extent the increased peak I_{Na} by ACO and MACO contributes to arrhythmic APs.

The significance of the $I_{Na/K}$ in generating repolarization abnormalities during APs has not been seriously explored in previous studies. A previous study showed that $I_{Na/K}$ inhibition

contributed to APD shortening, RMP elevation and DAD formation [24, 29], and $I_{Na/K}$ inhibition is common in diseases such as heart failure and ischemia [12]. In the current study, we found that the effects of ACO and MACO on APs at least partially overlapped with those of NKP inhibitors, suggesting that ACO and MACO could function as NKP inhibitors. This notion was further supported by the observation that ACO and MACO inhibited OUA-sensitive $I_{Na/K}$ currents.

The leaves of *Aconitum kusnezoffii* contain approximately 2–5 times more MACO than ACO [34]. Although MACO has a more potent pharmacological effect [14, 15], ACO appears to be more relevant to the arrhythmogenic effect of *Aconitum*, which has been well-known for a long time and established for modeling arrhythmia in animals. However, our ECG and AP data from guinea pigs in vivo and from ventricular myocytes in vitro indicate that MACO possesses similar yet more potent arrhythmogenic effects than ACO. The similar, if not the same, arrhythmogenic effects between ACO and MACO indicate that they share identical mechanisms in vivo and in vitro. Thus, MACO could replace ACO to generate an arrhythmia model, especially a model of more serious arrhythmia.

A low concentration of TTX (2 μ M) was adopted to minimize the effects of ACO and MACO on APs, as TTX significantly and reversibly shortened APD_{95} at 6 μ M [35, 36] but had almost no obvious effects on APD_{95} at 2 μ M [27]. Our results demonstrated that the changes in APs caused by ACO and MACO were largely abolished by TTX. This result was consistent with the findings of Ono et al., who demonstrated that TTX delayed the onset time of the arrhythmogenic effect of ACO and reduced mortality in mice [37]. In addition, OUA (0.1 μ M) was adopted to inhibit the NKP [38] while causing fewer arrhythmic AP changes [37]. The changes in APs caused by ACO and MACO were largely abolished by OUA.

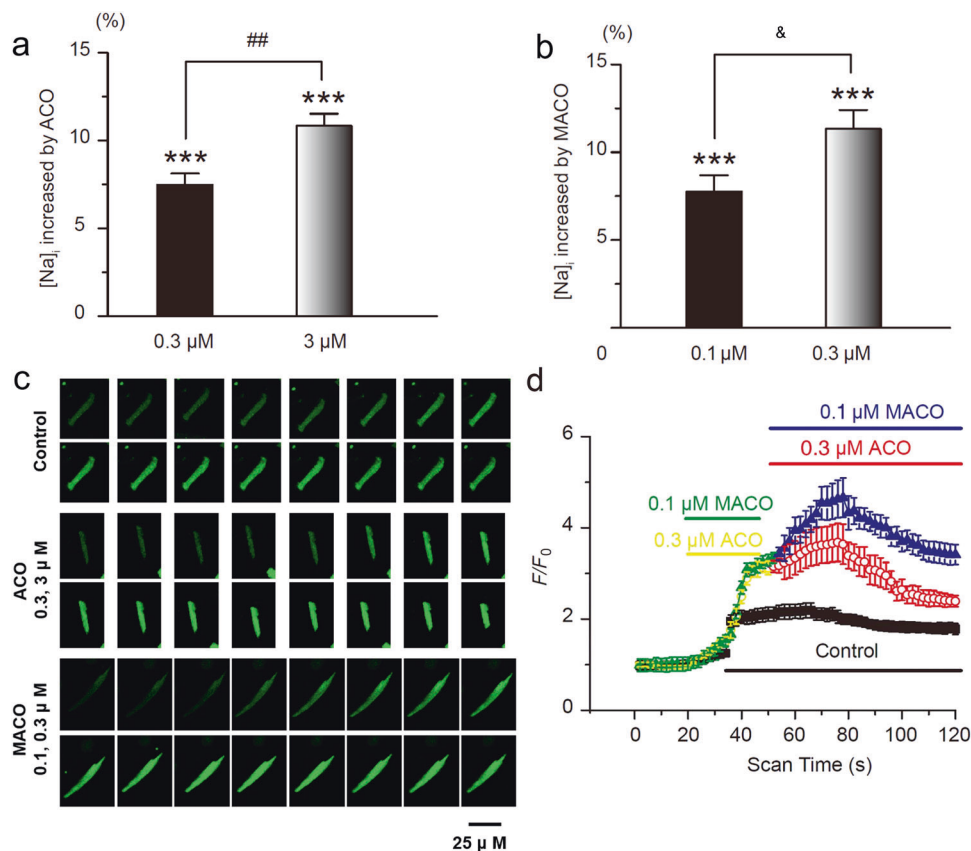


Fig. 8 Effects of ACO and MACO on $[Na]_i$ and $[Ca^{2+}]_i$ in guinea pig ventricular myocytes. **a, b** ACO and MACO increased $[Na]_i$ in a concentration-dependent manner in guinea pig ventricular myocytes. **c** Representative fluorescent images of ventricular myocytes loaded with Fluo-4/AM before (control) and after the addition of ACO (0.3 or 3 μM) or MACO (0.1 or 3 μM). In the control group, images 1–3 and 4–16 represent before and after the addition of high- K^+ solution to the extracellular solution. In the ACO or MACO group, images 1–3 represent before the addition of high- K^+ solution, and images 4–8 and 9–16 represent before and after the addition of high- K^+ solution containing ACO (0.3, 3 μM) or MACO (0.1, 0.3 μM). The images were captured at 1 frame per 8 s, and then IF was analyzed. **d** Changes in $[Ca^{2+}]_i$ by ACO and MACO are expressed as F/F_0 . There were seven cells from three guinea pig hearts in each group. *** $P < 0.001$, vs. control group; ## $P < 0.01$, vs. 0.3 μM ACO group; & $P < 0.05$, vs. 0.1 μM MACO group.

Similar results were reported by Raymod et al., who demonstrated that simultaneous intravenous administration of OUA truly converted atrial tachycardia induced by ACO to normal sinus rhythm in dogs [39]. These data reveal that both TTX and OUA act as antidotes for *Aconitum*-induced arrhythmia. Further experiments are needed to explore this question in multiple species.

Both ACO and MACO were noted in the present study to shorten APDs in cardiomyocytes of guinea pigs, and this finding was consistent with our previous studies both in the papillary muscle of guinea pigs [40] and in human induced pluripotent stem cells (hiPSC-CMs) [10]. NKP inhibition identified in the current study may contribute to this effect, and it was consistent with a previous report that NKP inhibition was involved in shortening APDs [24, 29]. More experiments are needed in the future.

One limitation of the current study is that all the experiments were performed at room temperature. The cells were exposed to an extracellular temperature that was not well controlled for a long duration of the experiment, and the direct effect of temperature on this study was the variation in APD values in the control group in different batches. In fact, the varied AP value of the control group at different temperatures was also confirmed by other researchers [41–43]. However, since the comparison was performed in the same group before and after the drug treatment, the tendency of the effect change in the presence of the drug was consistent (Supplementary Fig. S1). Therefore, the temperature variation does not affect the result. Nevertheless, it is necessary to observe the effects of the drugs on AP configuration at

physiological temperature. Another limitation is that the ventricular myocytes used in this study were from untreated (with ACO or MACO) guinea pigs. It would be interesting to measure the electrophysiological properties in ventricular myocytes from treated animals. Further studies are needed to clarify these questions.

CONCLUSION

In summary, the present study demonstrated that ACO and MACO can induce various kinds of ventricular arrhythmias in guinea pigs in vivo and in vitro, which are attributed to at least partially to the increase in peak I_{Na} through the acceleration of sodium channel activation and NKP inhibition. The effect of MACO appears to be more potent than that of ACO. This new understanding of the cellular electrophysiological mechanism of ACO-induced arrhythmias may improve safety considerations in the treatment of clinical conditions with *Aconitum*, benefit the development of new targeted treatments for *Aconitum*-induced cardiotoxicity events and facilitate the proper usage of ACO-induced arrhythmia models.

ACKNOWLEDGEMENTS

This study was supported by the National Natural Science Foundation of China (NSFC, 81773828, 81770407, 81903730), the Natural Science Foundation of Hebei Province

(C2011206145, H2018206297, C2018206277, H2019423130), and the Research Foundation of Education Bureau of Hebei Province (BJ2019037).

AUTHOR CONTRIBUTIONS

SWS, CW, and HMW designed the research. XCW, QZJ, YLY, HDW, CTL, XDM, XYC, QFM, and BCG performed the experiments. XCW, YLY, QZJ, HCG, and SWS analyzed the data. XCW, SWS, HMW, and XDM wrote the paper and prepared all of the figures. All authors reviewed and approved the final version of the paper.

ADDITIONAL INFORMATION

The online version of this article (<https://doi.org/10.1038/s41401-020-0467-6>) contains supplementary material, which is available to authorized users.

Competing interests: The authors declare no competing interests.

REFERENCES

- Singhuber J, Zhu M, Prinz S, Kopp B. *Aconitum* in traditional Chinese medicine: a valuable drug or an unpredictable risk? *J Ethnopharmacol.* 2009;126:18–30.
- Lin MW, Wang YJ, Liu SL, Lin AA, Lo YC, Wu SN. Characterization of aconitine-induced block of delayed rectifier K^+ current in differentiated NG108-15 neuronal cells. *Neuropharmacology.* 2008;54:912–23.
- Chan TY. Aconite poisoning. *Clin Toxicol.* 2009;47:279–85.
- Bartosova L, Novak F, Bebarova M, Frydrych M, Brunclik V, Opatrilova R, et al. Antiarrhythmic effect of newly synthesized compound 44Bu on model of aconitine-induced arrhythmia—compared to lidocaine. *Eur J Pharmacol.* 2007;575:127–33.
- Amran MS, Hashimoto K, Homma N. Effects of sodium-calcium exchange inhibitors, KB-R7943 and SEA0400, on aconitine-induced arrhythmias in guinea pigs in vivo, in vitro, and in computer simulation studies. *J Pharmacol Exp Ther.* 2004;310:83–9.
- Li Y, Tu D, Xiao H, Du Y, Zou A, Liao Y, et al. Aconitine blocks HERG and $Kv1.5$ potassium channels. *J Ethnopharmacol.* 2010;131:187–95.
- Wang YJ, Chen BS, Lin MW, Lin AA, Peng H, Sung RJ, et al. Time-dependent block of ultrarapid-delayed rectifier K^+ currents by aconitine, a potent cardiotoxin, in heart-derived H9c2 myoblasts and in neonatal rat ventricular myocytes. *Toxicol Sci.* 2008;106:454–63.
- Wright SN. Comparison of aconitine-modified human heart (hH1) and rat skeletal (mu1) muscle Na^+ channels: an important role for external Na^+ ions. *J Physiol.* 2002;538:759–71.
- Sun GB, Sun H, Meng XB, Hu J, Zhang Q, Liu B, et al. Aconitine-induced Ca^{2+} overload causes arrhythmia and triggers apoptosis through p38 MAPK signaling pathway in rats. *Toxicol Appl Pharmacol.* 2014;279:8–22.
- Wu J, Wang X, Chung YY, Koh CH, Liu Z, Guo H, et al. L-type calcium channel inhibition contributes to the proarrhythmic effects of aconitine in human cardiomyocytes. *PLoS One.* 2017;12:e0168435.
- Zhou YH, Piao XM, Liu X, Liang HH, Wang LM, Xiong XH, et al. Arrhythmogenesis toxicity of aconitine is related to intracellular Ca^{2+} signals. *Int J Med Sci.* 2013;10:1242–9.
- Britton OJ, Bueno-Orovio A, Virag L, Varro A, Rodriguez B. The electrogenic Na^+/K^+ Pump is a key determinant of repolarization abnormality susceptibility in human ventricular cardiomyocytes: a population-based simulation study. *Front Physiol.* 2017;8:278.
- Guo D, Jenkinson S. Simultaneous assessment of compound activity on cardiac $Nav1.5$ peak and late currents in an automated patch clamp platform. *J Pharmacol Toxicol Methods.* 2018;99:106575.
- Mitamura M, Horie S, Sakaguchi M, Someya A, Tsuchiya S, Van de Voorde J, et al. Mesaconitine-induced relaxation in rat aorta: involvement of Ca^{2+} influx and nitric-oxide synthase in the endothelium. *Eur J Pharmacol.* 2002;436:217–25.
- Ogura J, Mitamura M, Someya A, Shimamura K, Takayama H, Aimi N, et al. Mesaconitine-induced relaxation in rat aorta: role of Na^+/Ca^{2+} exchangers in endothelial cells. *Eur J Pharmacol.* 2004;483:139–46.
- Liu QH, Li XL, Xu YW, Lin YY, Cao JM, Wu BW. A novel discovery of I_{K1} channel agonist: zacopride selectively enhances I_{K1} current and suppresses triggered arrhythmias in the rat. *J Cardiovasc Pharmacol.* 2012;59:37–48.
- Wang YH, Shi CX, Dong F, Sheng JW, Xu YF. Inhibition of the rapid component of the delayed rectifier potassium current in ventricular myocytes by angiotensin II via the AT1 receptor. *Br J Pharmacol.* 2008;154:429–39.
- Park MH, Park WS, Jo SH. Acute alteration of cardiac ECG, action potential, I_{K1} and the human ether-a-go-go-related gene (hERG) K^+ channel by PCB 126 and PCB 77. *Toxicol Appl Pharmacol.* 2012;262:60–9.
- Wang C, Hennessey JA, Kirkton RD, Wang C, Graham V, Puranam RS, et al. Fibroblast growth factor homologous factor 13 regulates Na^+ channels and conduction velocity in murine hearts. *Circ Res.* 2011;109:775–82.
- Yuill KH, Convery MK, Dooley PC, Doggrell SA, Hancox JC. Effects of BDF 9198 on action potentials and ionic currents from guinea-pig isolated ventricular myocytes. *Br J Pharmacol.* 2000;130:1753–66.
- Bers DM, Barry WH, Despa S. Intracellular Na^+ regulation in cardiac myocytes. *Cardiovasc Res.* 2003;57:897–912.
- Wang X, Tang H, Wei EQ, Wang Z, Yang J, Yang R, et al. Conditional knockout of Fgf13 in murine hearts increases arrhythmia susceptibility and reveals novel ion channel modulatory roles. *J Mol Cell Cardiol.* 2017;104:63–74.
- Hamada K, Matsuura H, Sanada M, Toyoda F, Omatsu-Kanbe M, Kashiwagi A, et al. Properties of the Na^+/K^+ pump current in small neurons from adult rat dorsal root ganglia. *Br J Pharmacol.* 2003;138:1517–27.
- Lee SY, Lee CO. Inhibition of Na^+/K^+ pump and L-type Ca^{2+} channel by glibenclamide in guinea pig ventricular myocytes. *J Pharmacol Exp Ther.* 2005;312:61–8.
- Wang Y, Gao J, Mathias RT, Cohen IS, Sun X, Baldo GJ. alpha-Adrenergic effects on Na^+/K^+ pump current in guinea-pig ventricular myocytes. *J Physiol.* 1998;509:117–28.
- Li C, Zou R, Zhang H, Wang Y, Qiu B, Qiu S, et al. Upregulation of phosphoinositide 3-kinase prevents sunitinib-induced cardiotoxicity in vitro and in vivo. *Arch Toxicol.* 2019;93:1697–712.
- Jakob H, Nawrath H. Tetrodotoxin slightly shortens action potential duration in ventricular but not in atrial heart muscle. *Experientia.* 1988;44:16–7.
- Antzelevitch C, Nesterenko V, Shryock JC, Rajamani S, Song Y, Belardinelli L. The role of late I_{Na} in development of cardiac arrhythmias. *Handb Exp Pharmacol.* 2014;221:137–68.
- Glitsch HG. Electrophysiology of the sodium-potassium-ATPase in cardiac cells. *Physiol Rev.* 2001;81:1791–826.
- Levi AJ, Dalton GR, Hancox JC, Mitcheson JS, Issberner J, Bates JA, et al. Role of intracellular sodium overload in the genesis of cardiac arrhythmias. *J Cardiovasc Electrophysiol.* 1997;8:700–21.
- Gadsby DC, Nakao M. Steady-state current-voltage relationship of the Na/K pump in guinea pig ventricular myocytes. *J Gen Physiol.* 1989;94:511–37.
- Lewalle A, Niederer SA, Smith NP. Species-dependent adaptation of the cardiac Na^+/K^+ pump kinetics to the intracellular Na^+ concentration. *J Physiol.* 2014;592:5355–71.
- Song Y, Shryock JC, Belardinelli L. An increase of late sodium current induces delayed afterdepolarizations and sustained triggered activity in atrial myocytes. *Am J Physiol Heart Circ Physiol.* 2008;294:H2031–9.
- Zan K, Wangjie CR, Lu J, Guo LN, Zheng J, Ma SC. Content determination of four diester diterpenoid alkaloids in leaves of *Aconitum kusnezoffii* by HPLC. *Zhongguo Zhong Yao Za Zhi.* 2018;43:766–71.
- Kiyosue T, Arita M. Late sodium current and its contribution to action potential configuration in guinea pig ventricular myocytes. *Circ Res.* 1989;64:389–97.
- Song Y, Belardinelli L. Basal late sodium current is a significant contributor to the duration of action potential of guinea pig ventricular myocytes. *Physiol Rep.* 2017;5:e13295.
- Ono T, Hayashida M, Tezuka A, Hayakawa H, Ohno Y. Antagonistic effects of tetrodotoxin on aconitine-induced cardiac toxicity. *J Nippon Med Sch.* 2013;80:350–61.
- Wu Y, Wang L, Ma J, Song Y, Zhang P, Luo A, et al. Protein kinase C and Ca^{2+} -calmodulin-dependent protein kinase II mediate the enlarged reverse I_{NCX} induced by ouabain-increased late sodium current in rabbit ventricular myocytes. *Exp Physiol.* 2015;100:399–409.
- Lipicky RJ, Donovan TJ, Traycoff RB. Ouabain conversion of aconitine-induced atrial tachycardias. *Life Sci.* 1971;10:1021–7.
- Chen X, Guo H, Li Q, Zhang Y, Liu H, Zhang X, et al. Protective effect of berberine on aconite induced myocardial injury and the associated mechanisms. *Mol Med Rep.* 2018;18:4468–76.
- Vornanen M. The temperature dependence of electrical excitability in fish hearts. *J Exp Biol.* 2016;219:1941–52.
- Hyun NG, Hyun KH, Lee K, Kaang BK. Temperature dependence of action potential parameters in Aplysia neurons. *Neurosignals.* 2012;20:252–64.
- Abramochkin DV, Haverinen J, Mitenkov YA, Vornanen M. Temperature and external K^+ dependence of electrical excitation in ventricular myocytes of cod-like fishes. *J Exp Biol.* 2019;222:jeb193607.